

# Distinct Signatures For Coulomb Blockade and Aharonov-Bohm Interference in Electronic Fabry-Pérot Interferometers

Yiming Zhang,<sup>1</sup> D. T. McClure,<sup>1</sup> E. M. Levenson-Falk,<sup>1</sup> C. M. Marcus,<sup>1</sup> L. N. Pfeiffer,<sup>2</sup> and K. W. West<sup>2</sup>

<sup>1</sup>*Department of Physics, Harvard University, Cambridge, Massachusetts 02138, USA*

<sup>2</sup>*Bell Laboratories, Alcatel-Lucent Technologies, Murray Hill, NJ 07974, USA*

(Dated: June 5, 2021)

Two distinct types of magnetoresistance oscillations are observed in two electronic Fabry-Pérot interferometers of different sizes in the integer quantum Hall regime. Measuring these oscillations as a function of magnetic field and gate voltages, we observe three signatures that distinguish the two types. The oscillations observed in a  $2.0\ \mu\text{m}^2$  device are understood to arise from the Coulomb blockade mechanism, and those observed in an  $18\ \mu\text{m}^2$  device from the Aharonov-Bohm mechanism. This work clarifies, provides ways to distinguish, and demonstrates control over, these distinct physical origins of resistance oscillations seen in electronic Fabry-Pérot interferometers.

Mesoscopic electronics can exhibit wave-like interference effects [1, 2, 3, 4], particle-like charging effects [5], or a complex mix of both [6]. Experiments over the past two decades have investigated the competition between wave and particle properties [7], as well as regimes where they coexist [6, 8, 9, 10]. The electronic Fabry-Pérot interferometer (FPI)—a planar two-contact quantum dot operating in the quantum Hall regime—is a system where both interference and Coulomb interactions can play important roles. This device has attracted particular interest recently due to predicted signatures of fractional [11] and non-Abelian [12, 13, 14] statistics. The interpretation of experiments, however, is subtle, and must account for the interplay of charging and interference effects in these coherent confined structures.

Early measurements by van Wees *et al.* [15] demonstrated resistance oscillations as a function of magnetic field in an electronic FPI, with an interpretation given in terms of Aharonov-Bohm (AB) interference of edge states. More recently, experimental [16, 17, 18, 19] and theoretical [20, 21, 22] investigations indicate that Coulomb interaction plays a critical role in these previously observed conductance oscillations—as a function of both magnetic field and electrostatic gate voltage—suggesting an interpretation in terms of field- or gate-controlled Coulomb blockade (CB). Other recent experiments studying fractional charge and statistics in FPI's [23, 24] interpret resistance oscillations as arising from AB interference while taking the gate-voltage period as indicating a change of a quantized charge.

In this Letter, we report oscillations of resistance as a function of perpendicular magnetic field,  $B$ , and gate voltage in FPI's of different sizes. Oscillations in the smaller ( $2.0\ \mu\text{m}^2$ ) device are consistent with the interacting (CB) interpretation, while those in the larger ( $18\ \mu\text{m}^2$ ) device are consistent with noninteracting AB interference. Specifically, three signatures that distinguish the two types of oscillations are presented: The magnetic field period is roughly proportional to  $B$  for CB, but field-independent for AB; The gate-voltage pe-

riod is field-independent for CB, but proportional to  $1/B$  for AB; Resistance stripes in the two-dimensional plane of  $B$  and gate voltage have a positive (negative) slope in the CB (AB) regime.

The devices were fabricated on a high-mobility two-dimensional electron gas (2DEG) residing in a 30 nm wide GaAs/AlGaAs quantum well 200 nm below the chip surface, with Si  $\delta$ -doping layers 100 nm below and above the quantum well. The mobility is  $\sim 2,000\ \text{m}^2/\text{Vs}$  measured in the dark, and the density is  $2.6 \times 10^{15}\ \text{m}^{-2}$ . Surface gates that define the FPI's are patterned using electron-beam lithography on wet-etched Hall bars [see Fig. 1(a)]. These gates come in from top left and bot-

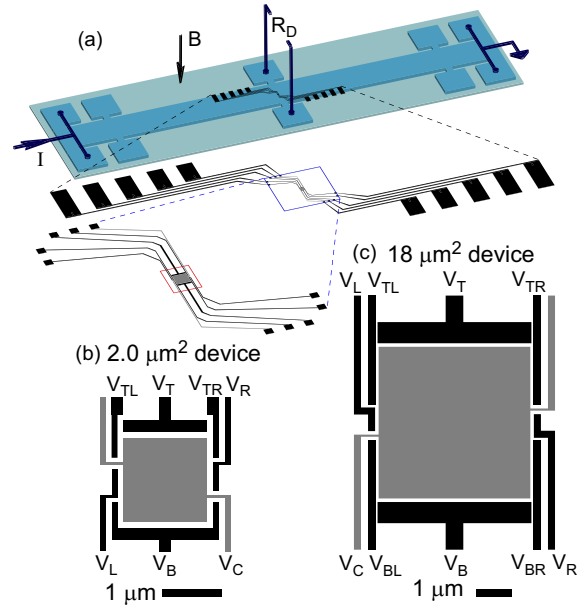


FIG. 1: Measurement setup and devices. (a) Diagram of the wet-etched Hall bar, surface gates, and measurement configuration. Diagonal resistance,  $R_D$ , is measured directly across the Hall bar, with current bias,  $I$ . Subsequent zoom-ins of the surface gates are also shown; the red box encloses the detailed gate layouts for the device shown in (c). (b,c) Gate layouts for the  $2.0\ \mu\text{m}^2$  and  $18\ \mu\text{m}^2$  devices, respectively. The areas quoted refer to those under  $V_C$ .

tom right, converging near the middle of the Hall bar. Figures 1(b) and 1(c) show gate layouts for the  $2.0 \mu\text{m}^2$  and  $18 \mu\text{m}^2$  interferometers. All gate voltages except  $V_C$  are set around  $\sim -3 \text{ V}$  (depletion occurs at  $\sim -1.6 \text{ V}$ ). Voltages,  $V_C$ , on the center gates are set near  $0 \text{ V}$  to allow fine tuning of density and area.

Measurements are made using a current bias  $I = 400 \text{ pA}$ , with  $B$  oriented into the 2DEG plane as shown in Fig. 1(a). The diagonal resistance,  $R_D \equiv dV_D/dI$  is related to the dimensionless conductance of the device  $g = (h/e^2)/R_D$  [25]. Here,  $V_D$  is the voltage difference between edge states entering from the top right and bottom left of the device. Figure 2(a) shows  $R_D$  as a function of  $B$ , displaying several quantized integer plateaus. Figures 2(b) and 2(c) show the zoom-ins below the  $g = 1$  and  $2$  plateaus, respectively, displaying oscillations in  $R_D$  as a function of  $B$ , with periods  $\Delta B = 2.1 \text{ mT}$  and  $1.1 \text{ mT}$ . This  $\Delta B$  of  $2.1 \text{ mT}$  corresponds to one flux quantum,  $\phi_0 \equiv h/e$ , through an area  $A = 2.0 \mu\text{m}^2$ ; hence  $1.1 \text{ mT}$  corresponds to  $\phi_0/2$  through about the same area. Figure 2(d) shows  $\Delta B$ , measured wherever oscillations appear, as a function of  $B$ ; a linear fit constrained to pass through the origin shows that  $\Delta B$  is almost proportional to  $B$ . Zoom-ins of the data in Fig. 2(d) below the  $g = 1$  and  $2$  plateaus are shown in Figs. 2(e) and 2(f) and clearly show that for both cases, the data are flatter than the linear fit.

This approximate proportionality between  $\Delta B$  and  $B$  is inconsistent with simple AB oscillations, which would give a constant  $\Delta B$  corresponding to one flux quantum through the area of the device. However, a recent theoretical analysis that accounts for Coulomb interaction between edge states found that for  $f_C$  occupied Landau levels (LL's) in the two constrictions,  $\Delta B = (\phi_0/A)/f_C$  for weak forward tunneling of the  $(f_C + 1)^{\text{th}}$  level, and  $\Delta B = (\phi_0/A)/(f_C - 1)$  for weak backscattering of the  $f_C^{\text{th}}$  level [21]. Interpolating between these two limits, we expect when the device conductance,  $g$ , is anywhere between  $f_0$  and  $f_0 + 1$ , that  $\Delta B = (\phi_0/A)/f_0$ . Here,  $f_0$  is the number of fully occupied LL's passing through the device (represented by different colored backgrounds in Fig. 2 for  $f_0 = 1$  to  $4$ ). Note that this model requires the  $(f_0 + 1)^{\text{th}}$  LL to be partially filled in both constrictions; otherwise, no oscillations are expected.

In this picture, on the riser of  $R_D$  where  $f_0 < g < f_0 + 1$ , the  $(f_0 + 1)^{\text{th}}$  and higher LL's will form a quasi-isolated island inside the device that will give rise to Coulomb blockade effects for sufficiently high field and large charging energy,

$$E_C = \frac{e^2}{2C} (f_0 \cdot BA/\phi_0 + N - \alpha V_{\text{gate}})^2,$$

where  $N$  is the number of electrons on the island,  $C$  is the total capacitance, and  $\alpha$  is the lever-arm associated with gate voltage  $V_{\text{gate}}$  [21]. The magnetic field couples electrostatically to the island through the underlying LL's:

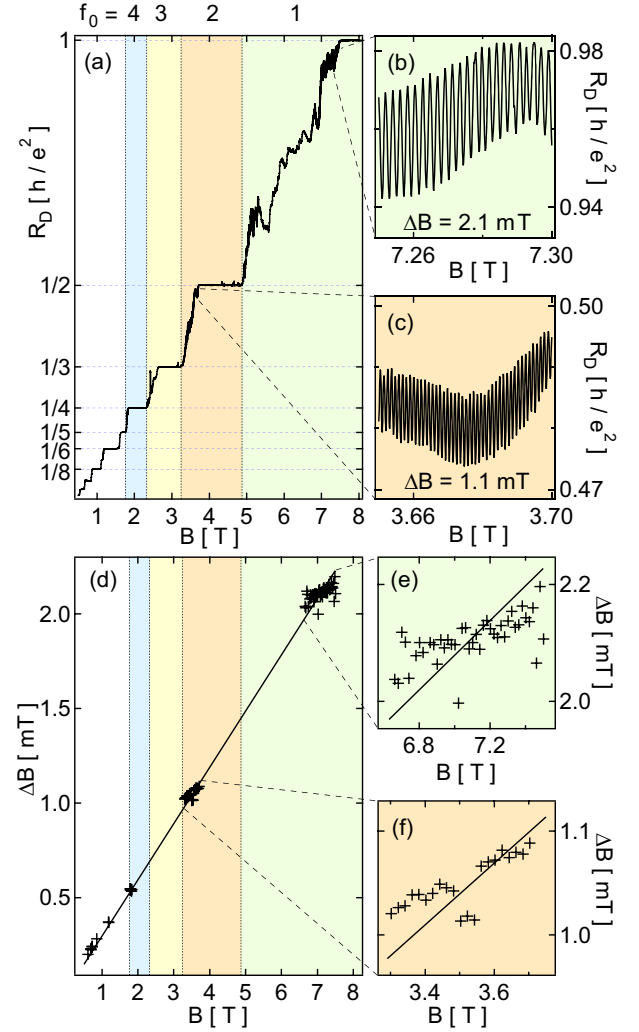


FIG. 2: Oscillations in  $R_D$  as a function of magnetic field,  $B$ , for the  $2.0 \mu\text{m}^2$  device. (a)  $R_D$  as a function of  $B$ , showing well-quantized integer plateaus. Different colored backgrounds indicate different numbers of fully-occupied LL's,  $f_0$ , through the device. (b, c) Zoom-ins of the data in (a), at  $f_0 = 1$  and  $2$ , respectively, showing oscillations in  $R_D$ , and their  $B$  periods,  $\Delta B$ . (d) Observed  $\Delta B$  as a function of  $B$ , with a straight-line fit through the origin. (e, f) Zoom-ins of the data in (d) at  $f_0 = 1$  and  $2$ , respectively.

when  $B$  increases by  $\phi_0/A$ , the number of electrons in each of the  $f_0$  underlying LL's will increase by one. These LL's will act as gates to the isolated island: Coulomb repulsion favors a constant total electron number inside the device, so  $N$  will decrease by  $f_0$  for every  $\phi_0/A$  change in  $B$ , giving rise to  $f_0$  resistance oscillations. This picture not only explains the approximate proportionality of  $\Delta B$  to  $B$ , because  $B \sim 1/f_0$ , but also explains small deviations from it. As seen in Figs. 2(e) and 2(f), the  $\Delta B$  data is flatter than the straight-line fit. This picture actually predicts a constant  $\Delta B$  for a given  $f_0$ , and the observed increase of  $\Delta B$  can be accounted for as the device area shrinks slightly at higher fields.

Motivated by this picture, in Fig. 3(a) we show the

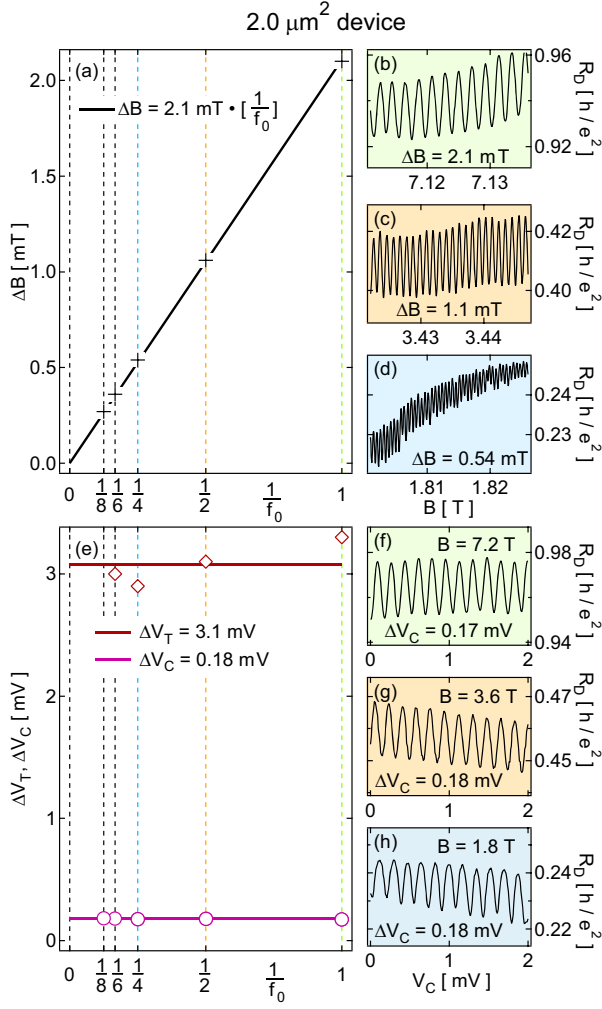


FIG. 3: Magnetic field and gate voltage periods at various  $f_0$ , for the  $2.0 \mu\text{m}^2$  device. (a)  $\Delta B$  as a function of  $1/f_0$ , and a best-fit line constrained through the origin. (b-d)  $R_D$  oscillations as a function of  $B$ , at  $f_0 = 1, 2$ , and  $4$ , respectively. (e)  $\Delta V_T$  (diamonds) and  $\Delta V_C$  (circles) as a function of  $1/f_0$ , and their averages indicated by horizontal lines. (f-h)  $R_D$  oscillations as a function of  $V_C$ , at  $f_0 = 1, 2$ , and  $4$ , respectively.

average  $\Delta B$  at each  $1/f_0$ , and a straight-line fit constrained through the origin, demonstrating the expected relationship  $\Delta B = (\phi_0/A)/f_0$ , with  $A = 2.0 \mu\text{m}^2$ . Further evidence of the CB mechanism in the  $2.0 \mu\text{m}^2$  device is found in the resistance oscillations as a function of gate voltages. Figures 3(f-h) show  $R_D$  as a function of center gate voltage  $V_C$ , for  $f_0 = 1, 2$  and  $4$ , respectively. Figure 3(e) summarizes gate voltage periods  $\Delta V_T$  and  $\Delta V_C$  at various  $f_0$ , and shows they are independent of  $f_0$ . This behavior is consistent with the CB mechanism, as gate-voltage periods are determined by the charging energy and lever arm to the gate, both of which are approximately independent of  $B$ .

Having identified CB as the dominant mechanism for resistance oscillations in the  $2.0 \mu\text{m}^2$  device, we fabricated and measured an  $18 \mu\text{m}^2$  device, an order of

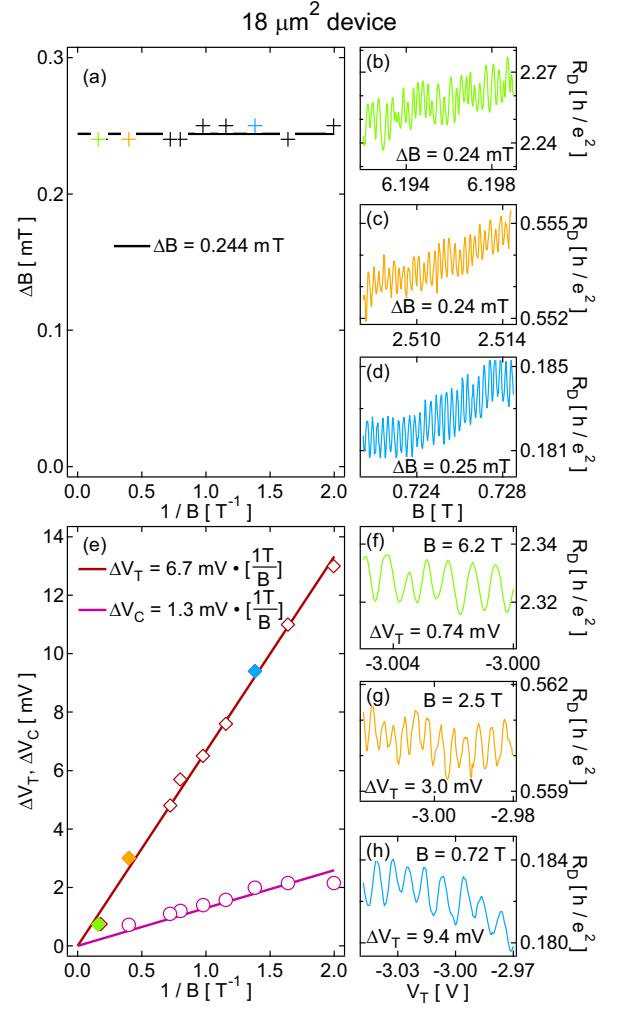


FIG. 4: Magnetic field and gate voltage periods at various  $B$ , for the  $18 \mu\text{m}^2$  device. (a)  $\Delta B$  as a function of  $1/B$ , and their average indicated by a horizontal line. (b-d)  $R_D$  oscillations as a function of  $B$ , over three magnetic field ranges. (e)  $\Delta V_T$  (diamonds) and  $\Delta V_C$  (circles) as a function of  $1/B$ , and best-fit lines constrained through the origin. (f-h)  $R_D$  oscillations as a function of  $V_T$ , at  $B = 6.2 \text{ T}, 2.5 \text{ T}$ , and  $0.72 \text{ T}$ , respectively.

magnitude larger in size, hence an order of magnitude smaller in charging energy. The center gate covering the whole interferometer, not present in previous experiments [15, 16, 18, 19], also serves to reduce the charging energy. In this device,  $R_D$  as a function of  $B$  at three different fields is plotted in Figs. 4(b-d), showing nearly constant  $\Delta B$ . The summary of data in Fig. 4(a) shows that  $\Delta B$ , measured at 10 different fields ranging from  $0.5$  to  $6.2 \text{ T}$ , is indeed independent of  $B$ ; its average value of  $0.244 \text{ mT}$  corresponds to one  $\phi_0$  through an area of  $17 \mu\text{m}^2$ , close to the designed area. This is in contrast to the behavior observed in the  $2.0 \mu\text{m}^2$  device, and is consistent with AB interference. Gate voltage periods are also studied, as has been done in the  $2.0 \mu\text{m}^2$  device. Figures 4(f-h) show  $R_D$  as a function of  $V_T$  at three different fields, and Fig. 4(e) shows both  $\Delta V_T$  and  $\Delta V_C$  as

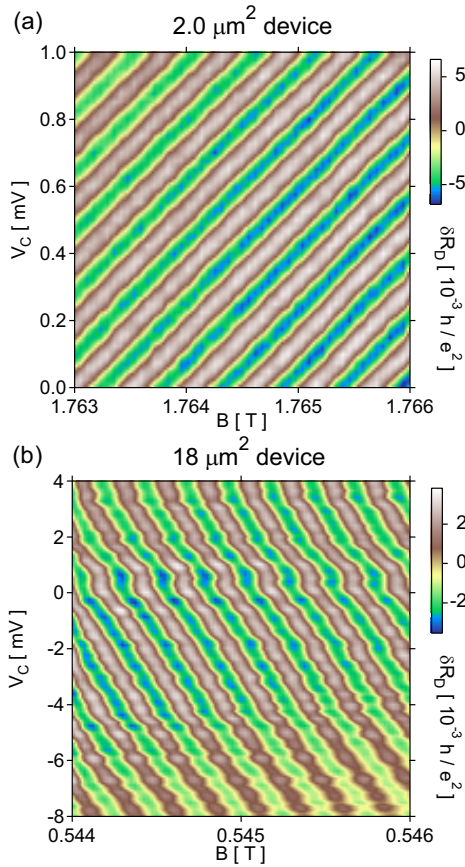


FIG. 5: (a)  $\delta R_D$ , i.e.  $R_D$  with a smooth background subtracted, as a function of  $B$  and  $V_C$ , for the  $2.0 \mu\text{m}^2$  device. (b) Same as in (a), but for the  $18 \mu\text{m}^2$  device.

a function of  $1/B$ . In contrast to the behavior observed in the  $2.0 \mu\text{m}^2$  device,  $\Delta V_T$  and  $\Delta V_C$  are no longer independent of  $B$ , but proportional to  $1/B$ . This behavior is consistent with AB interference, because the total flux is given by  $\phi = B \cdot A$  and the flux period is always  $\phi_0$ ; assuming that the area changes linearly with gate voltage, gate-voltage periods would scale as  $1/B$  for AB. Note that here, the gate voltage periods can vary smoothly with  $B$  and do not correspond to changes in a quantized charge.

As shown above, the magnetic field and gate voltage periods have qualitatively different  $B$  dependence in the  $2.0 \mu\text{m}^2$  and  $18 \mu\text{m}^2$  devices, the former consistent with CB, and the latter consistent with AB interference. Based on these physical pictures, one can make another prediction in which these two mechanisms will lead to opposite behaviors. In the CB case, increasing  $B$  increases the electron number in the underlying LL's, thus reducing the electron number in the isolated island via Coulomb repulsion. This is equivalent to applying more negative gate voltage to the device. On the other hand, for the AB case, increasing  $B$  increases the total flux through the interferometer, and applying more positive

gate voltage increases the area, thus also the total flux; therefore, higher  $B$  is equivalent to more positive gate voltage. As a result, if  $R_D$  is plotted in a plane of gate voltage and  $B$ , we expect stripes with a positive slope in the CB case and a negative slope in the AB case.

Figures 5(a,b) show  $R_D$  as a function of  $V_C$  and  $B$  for the  $2.0 \mu\text{m}^2$  and  $18 \mu\text{m}^2$  devices, respectively. As anticipated, the stripes from the  $2.0 \mu\text{m}^2$  device have a positive slope, consistent with the CB mechanism, while stripes from the  $18 \mu\text{m}^2$  device have a negative slope, consistent with AB interference. This difference can serve to determine the origin of resistance oscillations without the need to change magnetic field significantly.

We gratefully acknowledge J. B. Miller for device fabrication and discussion, R. Heeres for his work on the cryostat, and I. P. Radu, M. A. Kastner, B. Rosenow and B. I. Halperin for helpful discussions. This research is supported by Microsoft Corporation Project Q, IBM, NSF (DMR-0501796), and Harvard University.

- 
- [1] *Mesoscopic Phenomena in Solids*, edited by B. L. Altshuler, P. A. Lee, and R. A. Webb (North-Holland, Amsterdam, 1991).
  - [2] W. Liang *et al.*, Nature **411**, 665 (2001).
  - [3] Y. Ji *et al.*, Nature **422**, 415 (2003).
  - [4] P. Roulleau *et al.*, Phys. Rev. B **76**, 161309 (2007).
  - [5] L. P. Kouwenhoven *et al.*, in *Mesoscopic Electron Transport*, NATO ASI Series E **345** (1997).
  - [6] I. L. Aleiner, P. W. Brouwer, and L. I. Glazman, Physics Reports **358**, 309 (2002).
  - [7] E. Buks *et al.*, Nature **391**, 871 (1998).
  - [8] D. C. Glatthli *et al.*, Z. Phys. B **85**, 375 (1991).
  - [9] J. A. Folk *et al.*, Phys. Rev. Lett. **76**, 1699 (1996).
  - [10] S. M. Cronenwett *et al.*, Phys. Rev. Lett. **79**, 2312 (1997).
  - [11] C. de C. Chamon *et al.*, Phys. Rev. B **55**, 2331 (1997).
  - [12] A. Stern and B. I. Halperin, Phys. Rev. Lett. **96**, 016802 (2006).
  - [13] P. Bonderson, A. Kitaev, and K. Shtengel, Phys. Rev. Lett. **96**, 016803 (2006).
  - [14] R. Ilan, E. Grosfeld, and A. Stern, Phys. Rev. Lett. **100**, 086803 (2008).
  - [15] B. J. van Wees *et al.*, Phys. Rev. Lett. **62**, 2523 (1989).
  - [16] B. W. Alphenaar *et al.*, Phys. Rev. B **46**, 7236 (1992).
  - [17] R. P. Taylor *et al.*, Phys. Rev. Lett. **69**, 1989 (1992).
  - [18] F. E. Camino, W. Zhou, and V. J. Goldman, Phys. Rev. B **76**, 155305 (2007).
  - [19] M. D. Godfrey *et al.*, arXiv:0708.2448.
  - [20] M. W. C. Dharma-wardana, R. P. Taylor, and A. S. Sachrajda, Solid State Commun. **84**, 631 (1992).
  - [21] B. Rosenow and B. I. Halperin, Phys. Rev. Lett. **98**, 106801 (2007).
  - [22] S. Ihnatsenka and I. V. Zozoulenko, Phys. Rev. B **77**, 235304 (2008).
  - [23] F. E. Camino, W. Zhou, and V. J. Goldman, Phys. Rev. Lett. **95**, 246802 (2005); F. E. Camino, W. Zhou, and V. J. Goldman, Phys. Rev. Lett. **98**, 076805 (2007).
  - [24] R. L. Willett *et al.*, arXiv:0807.0221.
  - [25] J. B. Miller *et al.*, Nat. Phys. **3**, 561 (2007).